AIP Applied Physics Letters

The A-site driven phase transition procedure of (Pb0.97La0.02)(Zr0.42Sn0.40Ti0.18)O3 ceramics: An evidence from electronic structure variation

X. Chen, P. P Jiang, Z. H. Duan, Z. G. Hu, X. F. Chen, G. S. Wang, X. L. Dong, and J. H. Chu

Citation: Applied Physics Letters **103**, 192910 (2013); doi: 10.1063/1.4829757
View online: http://dx.doi.org/10.1063/1.4829757
View Table of Contents: http://scitation.aip.org/content/aip/journal/apl/103/19?ver=pdfcov
Published by the AIP Publishing

The A-site driven phase transition procedure of $(Pb_{0.97}La_{0.02})(Zr_{0.42}Sn_{0.40}Ti_{0.18})O_3$ ceramics: An evidence from electronic structure variation

X. Chen (陈啸),[1] P. P Jiang (姜鹏鹏),[1] Z. H. Duan (段志华),[1] Z. G. Hu (胡志高),[1,a)]
X. F. Chen (陈学锋),[2] G. S. Wang (王根水),[2] X. L. Dong (董显林),[2] and J. H. Chu (褚君浩)[1]
[1]*Key Laboratory of Polar Materials and Devices, Ministry of Education, Department of Electronic Engineering, East China Normal University, Shanghai 200241, China*
[2]*Key Laboratory of Inorganic Functional Materials and Devices, Shanghai Institute of Ceramics, Chinese Academy of Sciences, Shanghai 200050, China*

(Received 18 June 2013; accepted 28 October 2013; published online 8 November 2013)

The transition of $(Pb_{0.97}La_{0.02})(Zr_{0.42}Sn_{0.40}Ti_{0.18})O_3$ (PLZST) ceramic has been investigated by temperature-dependent X-ray diffraction (XRD) and spectroscopic ellipsometry (SE). The rhombohedral and tetragonal symmetries are confirmed by XRD analysis. Two interband transitions (E_{cp1} and E_{cp2}) located at about 3.7 and 5.2 eV can be derived from the second derivative of the complex dielectric functions using the standard critical point (SCP) model. Except for the negative temperature coefficient parts, the transitions present additional parts corresponding to appearance of the antiferroelectric (AFE) phase. The phenomena can be attributed to variation of the electronic structure during *A*-site driven phase transition. © *2013 AIP Publishing LLC*. [http://dx.doi.org/10.1063/1.4829757]

Owing to ferroelectric (FE), antiferroelectric (AFE), and other macroscopic properties (piezoelectric and pyroelectric), Pb-based ABO_3 perovskite materials have importance in applications as high-strain transducers or actuators, high-energy-storage capacitors, infrared detectors, and non-volatile random-access memory. In particular, the advantages can be obtained for compositions close to the morphotropic phase boundary (MPB).[1–3] These properties are mostly derived from the complex non-centrosymmetry microstructure of the materials.[4] To improve the properties for better application, mechanism study on determining the nature of anomalistic macroscopic properties becomes an interesting topic, which has attracted much attention in past decades. These macroscopic properties should originate from variation of microstructures and electronic band structures. Recently, Cohen revealed that the essential ferroelectricity is because of cross-gap hybridization between the occupied O 2*p* states and unoccupied Pb 6 *p* states.[5] Zhang *et al*. proposed a change in band gap of about 0.7 eV during the ferroelectric to paraelectric (PE) phase transition (PT) in $SrBi_2Ta_2O_9$.[6] However, both results were carried out by theoretical calculations and no experimental evidence was reported. Generally, the ferroelectricity and/or PT pattern may be related to the electronic band structure. Thus, experimental studies on the electronic structure during the PT process, especially for perovskite-type materials close to the MPB region, are desirable to clarify these physical behaviors.

Compared with the parent $Pb(ZrTi)O_3$ (PZT) system, $(PbLa)(ZrSnTi)O_3$ (PLZST) has a more complex phase diagram.[7] By applying external fields (temperature, electric, and pressure), even single composition PLZST could undergo not only a PE-FE transition but also a ferroelectric to antiferroelectric transition (FE-AFE).[8,9] For example, the P behavior of $(Pb_{0.97}La_{0.02})(Zr_{0.42}Sn_{0.40}Ti_{0.18})O_3$ ceramic was studied by means of transmission electron microscopy, polarization, and pyroelectric response. The high pyroelectric response (220×10^{-8} C cm^{-2} K^{-1}) and small thermal hysteresis (<1.5 °C) indicate that the material has promising applications.[9] Given the aforementioned physical interest and technical importance, it is necessary to investigate the electronic structure of PLZST to explore the potential applications.

Although the effect of La-substitution on the variation of the electronic structure of PLZST has been investigated by near-normal-incident unpolarized reflectance spectra,[13] optical temperature-dependent phase transition studies have not yet been performed. Compared with unpolarized reflectance spectra, spectroscopic ellipsometry (SE) has some advantages, such as two independently measured values recorded at each wavelength (amplitude ratio and phase shift difference) instead of one (amplitude), and the ability to remove the influence of surface roughness. Note that, the SE method for obtaining interband critical point (CP) energies has been applied to many semiconductor and dielectric materials.[10–12] In this letter, the variation of the electronic structure of PLZST has been investigated by temperature-dependent SE and the physical mechanism related to the PT pattern is discussed in detail.

The $(Pb_{0.97}La_{0.02})(Zr_{0.42}Sn_{0.40}Ti_{0.18})O_3$ ceramic was made by a traditional solid-state ceramic processing route.[13] The sample was sintered at 1300 °C for 1 h in air atmosphere. The sintering process was carried out in a lead rich environment to minimize lead volatilization. Then, the wafer with a diameter of 15 mm and a thickness of 1 mm was single-side polished. Because the SE experiment is quite sensitive to the surface roughness, the polishing process consisted of three steps: coarse grinding, fine grinding, and polishing. Before spectral measurements, the ceramic was rigorously cleaned

a)Author to whom correspondence should be addressed. Electronic mail: zghu@ee.ecnu.edu.cn. Tel.: +86-21-54345150. FAX: +86-21-54345119

in pure ethanol with an ultrasonic bath and rinsed several times with deionized water. The root-mean-square (rms) roughness was estimated to be about 5 nm by atomic force microscopy (AFM). Structural analysis was undertaken by temperature-dependent X-ray diffraction (XRD), which was carried out using a Bruker D8 Discover High Resolution XRD in the temperature range from 200 to 540 K (TCU100 Temperature Control Unit, LNC Nitrogen Suction Equipment, Anton Paar). Temperature-dependent SE experiments were performed by a vertical variable-angle near-infrared-ultraviolet SE (J.A. Woollam Co., Inc.) with an incident angle of 70°, working at the spectral range of 1.12–6 eV (206–1100 nm). An Instec Cell with the sample mounted inside was used to implement the temperature variation from 200 to 780 K with a precision of about ±1 K. It is worth noting that the SE experiment was recorded before the XRD scans to avoid sample defects, which can be caused by possible lead volatilization at high temperature.

Fig. 1 shows the results of the temperature-dependent XRD scans. The complete patterns are similar to previous results at room temperature.[13] The only difference is the additional peak located at ~52°, indicated by the black "diamond" in Fig. 1. This could be caused by the lead volatilization, because the melting point of PbO_2 of 563 K, is lower than the highest temperature applied in the SE experiment. Except for the additional peak, no secondary structure was observed. All diffraction patterns indicate a pure perovskite structure that is very similar to the patterns of the single crystal powder.[14] Fig. 1(b) shows the enlarged region located at ~45°, which is the characteristic PT region. The peak is singlet, indicating the rhombohedral-like phase at low temperature. A peak splitting tendency was readily observed, which suggests that the transition from the rhombohedral-like to the tetragonal-like phase occurs. Up to 380 K, there is a shoulder structure on the low angle side of the peak, showing the slow PT process. This indicates that the rhombohedral-like and tetragonal-like phases would coexist. At 420 K, the broad shoulder peak is located at the onset of changing into another peak. With further increasing temperature, two separate peaks are clearly distinguished from the XRD pattern at 480 and 540 K, respectively. Note that, the XRD results at different temperatures are in good agreement with the pyroelectric response of as-grown PLZST ceramic with the same stoichiometry, which showed a strong pyroelectric response peak at 115 °C (388 K).[8] Recently, Li *et al.* reported the orthorhombic symmetry in $(Pb_{0.97}La_{0.02})(Zr_{0.66}Sn_{0.27}Ti_{0.07})O_3$ single crystals, which is also found in many $PbZrO_3$-based antiferroelectrics.[15] Moreover, Li *et al.* suggested that the single crystal undergoes consecutive orthorhombic-rhombohedral-cubic PTs. Nevertheless, neither superlattice diffractions, which differentiate orthorhombic phase from tetragonal phase, nor a single peak located at ~45° at high temperatures, indicating the cubic phase, were observed in the present work. The former is mainly because of the complex phase diagram of the PZST family, which has obvious differences depending on the chemical ratios of Zr/Sn/Ti of the *B*-cation.[7] The latter can be attributed to the limited experimental temperature region for the XRD experiments. Note that the observation of the rhombohedral and tetragonal phases is in agreement with the phases separated by the aforementioned MPB.

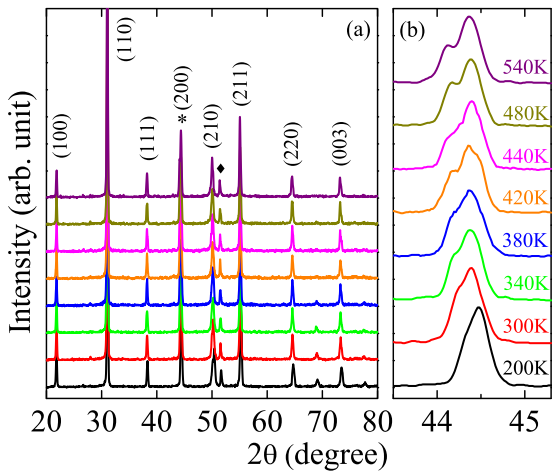

FIG. 1. (a) Temperature-dependent XRD profiles of PLZST ceramic. The black diamond "◆" indicates the additional peak of PbO_2 and the enlarged part of the (200) peak (indicated by the asterix "∗") is shown in (b). Note that an additional peak appears in (b) with increasing temperature.

Even though additional treatment steps were performed to reduce the surface roughness, the estimated roughness (~5 nm) may still affect the complex dielectric functions, especially for the estimation of the CPs. In the present work, a three-layer model (air/surface roughness/ceramic) was used to evaluate the complex dielectric function of the PLZST ceramic and the accurate thickness of the roughness layer. To model the surface roughness layer, the Brüggeman effective-medium approximation (EMA) with a mixture of the bulk material (50%) and voids (50%) was used. The complex dielectric function of PLZST was derived by the parametric model, which has been applied to PZT-based materials.[16] Two parametric oscillators, Psemi-M0 and Psemi-M3, were applied to estimate the complex dielectric function.[17] The comprehensive values of the parameters from the fitting spectra obtained at 200 K are listed in Table I. This fitting procedure was carried out with the WVASE32 software package (J.A. Woollam Co., Inc.). A weighted mean square error function was used. There is good agreement between the model and experimental Ψ and Δ spectra, as shown in Fig. 2(a). With the accurate thickness of the roughness layer (5.16 nm), the numerically inverted complex dielectric function (NICDF) of PLZST at every temperature could be directly calculated from the original experimental data. Compared with the complex dielectric function derived from the parametric model, the NICDF is more scientifically rigorous. For example, Fig. 2(b) shows the NICDF at three different temperatures. An obvious discrepancy can be observed in the complex dielectric functions, which can be attributed to the CP variation.

To obtain the accurate energy position of CP, fitting for the second derivative of the NICDF with the standard critical point (SCP) model was performed. The SCP model can be written as follows:

$$\frac{d^2\varepsilon}{dE^2} = n(n-1)A_m \exp(i\phi_m)(E - E_{cpm} + i\Gamma_m)^{n-2} \quad (n \neq 0),$$
$$\frac{d^2\varepsilon}{dE^2} = A_m \exp(i\phi_m)(E - E_{cpm} + i\Gamma_m)^{-2} \quad (n = 0), \qquad (1)$$

TABLE I. The best-fitting parameter values for PLZST at 200 K. The parameter *A*, *E*, *B*, *WL*, *WR*, *PL*, *PR*, *AL*, *AR*, *O2L*, and *O2R* is amplitude, center energy, broadening, width of left side absorption region, width of right side absorption region, control point position for left side, control point position for right side, control point amplitude for left side, control point amplitude for right side, second order polynomial factor for left side polynomials, and second order polynomial factor for right side polynomials, respectively. The "MSE" indicates root-mean-square fractional error for the fitting. Note that the 95% reliability of the fitting parameters is given in parentheses and the label "–" means that the parameter is fixed during the fitting process.

	Oscillator parameters												
Oscillator type	*A*	*E* (eV)	*B* (eV)	*WL* (eV)	*WR* (eV)	*PL*	*PR*	*AL*	*AR*	*O2L*	*O2R*	ε_1 Offset	Thickness of roughness layer (nm)	MSE
Psemi-M3	118	4.08	0.30	2.67	0	0.99	0.5	0.015	0.5	0	0	1.83 (0.17)	5.16 (0.23)	0.34
	(3)	(0.01)	(0.01)	(0.03)	–	(0.01)	–	(0.001)	–	–	–			
Psemi-M0	9.67	4.18	0.63	0	9.87	0.5	0.99	0.5	0.79	0	1			
	(0.70)	(0.22)	(0.02)	–	(0.28)	–	(0.05)	–	(0.53)	–	–			

where for the *m*th CP, A_m, E_{cpm}, Γ_m, ϕ_m are the amplitude, CP energy, broadening parameter, and the phase angle, respectively. Generally, the exponent *n* has values of -1, $-\frac{1}{2}$, 0, and $\frac{1}{2}$ for excitonic, one-, two-, and three-dimensional line shapes, respectively. In the present work, the parameter *n* was set to -1, which is consistent with the value for previously reported PZT-based materials.[16] Fig. 3 shows the second derivative of the NICDF and the best-fit curves at the six characteristic temperatures of 200, 320, 380, 420, 480, and 780 K, respectively. The fitted CP energies are indicated by arrows in each section of each specific temperature. For clarity, a set of the fitting parameters is listed in Table II. The consistency of the phase angle value (ϕ_m) for all temperatures can be seen ($\sim 20°$ for E_{cp1} and $\sim 16°$ for E_{cp2}), confirming the excitonic metamorphism of critical point line shapes (presented by $n = -1$) and the robustness of the fitting procedure.[18]

The CP energies obtained from the fitting calculations can be interpreted by the theoretical electronic band structures. Warren *et al.* suggested that the valence-band maximum (VBM) is a mixture of O *p* and Pb *s* states at *X* with $X_{4'v}$ symmetry. The conduction-band minimum (CBM) is composed of the *B* ion *d* states as X_{3c} at low Zr composition and switches to *A* ion Pb 6*p*-like states as X_{1c} with increase in the Zr content.[19] Furthermore, nearly O *p* states as $X_{5'v}$ at the top of Γ (Γ_{15v}) was proposed and three energy gaps corresponding to the transitions of $X_{4'v} \rightarrow X_{1c}$ (~ 3.9 eV), $X_{5'v} \rightarrow X_{3c}$ (~ 4.5 eV), and $X_{5'v} \rightarrow X_{1c}$ (~ 6.5 eV) were observed by Lee *et al.*[20] The theoretical results suggest that the substitution of Sn in the *B*-cation does not contribute much to the VBM and CBM because the *d* states of Sn are well below the valence band.[21] Thus, the obtained CP energies in the present work (E_{cp1} and E_{cp2}) can be uniquely assigned to the transitions of $X_{4'v} \rightarrow X_{1c}$ and $X_{5'v} \rightarrow X_{3c}$, respectively. Note that the third transition observed by Lee *et al.* is outside the present experimental photon energy range. It should be emphasized that all the aforementioned calculations were performed in the cubic symmetry, which should agree much better with the experimental results at high temperatures (~ 3.5 eV of E_{cp1} and ~ 5.2 eV of E_{cp2}) than at low temperatures. A smaller value of E_{cp1} can be explained by the substitution of La for Pb introducing an impurity band in the forbidden band of PZT, which leads to the decrease of the

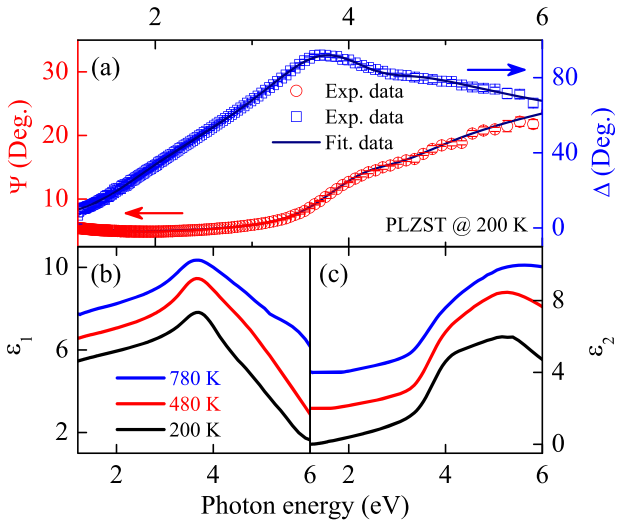

FIG. 2. (a) Experimental data with spectral errors (dots) and fitted curves (lines) of Ψ and Δ recorded at 200 K. The real part (b) and imaginary part (c) of numerically inverted complex dielectric functions are directly calculated from the original spectra by accounting for thickness of roughness layer at three different temperatures.

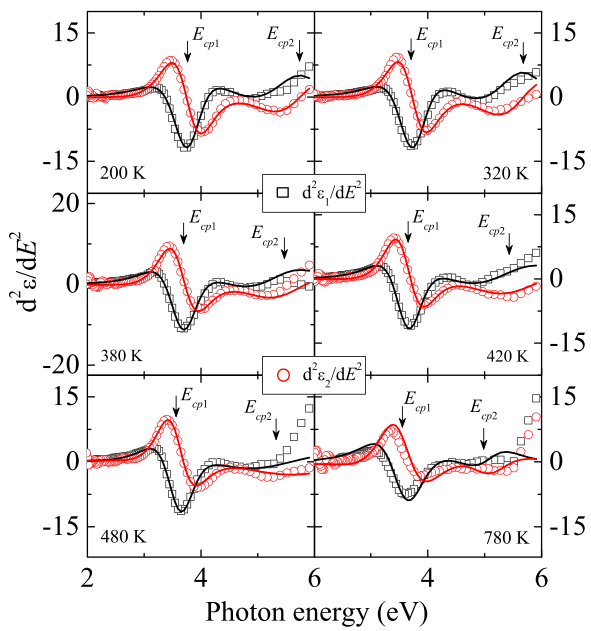

FIG. 3. Second derivative of the complex dielectric functions and the best fit at different temperatures. The critical point positions are marked with arrows. The dotted and solid lines are the experimental and fitting results, respectively.

TABLE II. The best-fitting parameters of the SCP model for PLZST ceramic extracted from the second derivative of the NICDF at different temperatures. The 95% reliability of the fitting parameters is given in parentheses.

	E_1				E_2			
Temperature (K)	A_1	E_{cp1} (eV)	Γ_1 (eV)	ϕ_1 (deg)	A_2	E_{cp2} (eV)	Γ_2 (eV)	ϕ_2 (deg)
200	1.32 (0.09)	3.76 (0.02)	0.62 (0.01)	20.5 (0.09)	3.13 (1.20)	5.72 (0.10)	1.09 (0.20)	17.2 (0.80)
250	1.29 (0.08)	3.76 (0.01)	0.59 (0.02)	20.3 (0.07)	3.53 (1.19)	5.70 (0.09)	1.15 (0.17)	16.8 (0.12)
300	1.29 (0.07)	3.74 (0.01)	0.60 (0.02)	20.2 (0.09)	3.21 (0.69)	5.64 (0.10)	1.10 (0.23)	16.8 (0.62)
320	1.20 (0.10)	3.73 (0.02)	0.59 (0.01)	20.5 (0.06)	3.11 (0.85)	5.71 (0.07)	1.11 (0.30)	16.9 (0.40)
340	1.34 (0.09)	3.74 (0.01)	0.60 (0.01)	20.3 (0.08)	3.30 (0.86)	5.62 (0.12)	1.06 (0.12)	17.0 (0.66)
360	1.47 (0.08)	3.69 (0.02)	0.63 (0.02)	20.2 (0.08)	2.19 (0.76)	5.49 (0.08)	0.86 (0.25)	17.1 (0.52)
380	1.16 (0.07)	3.66 (0.01)	0.59 (0.02)	20.1 (0.07)	4.65 (0.62)	5.48 (0.07)	1.36 (0.34)	16.4 (0.46)
400	1.25 (0.09)	3.62 (0.01)	0.60 (0.01)	20.0 (0.09)	6.91 (0.93)	5.41 (0.09)	1.66 (0.36)	16.4 (0.57)
420	1.10 (0.11)	3.63 (0.01)	0.59 (0.02)	20.2 (0.10)	7.60 (1.25)	5.45 (0.10)	1.62 (0.49)	16.1 (0.44)
440	1.27 (0.12)	3.61 (0.02)	0.61 (0.01)	20.5 (0.12)	4.66 (1.34)	5.27 (0.07)	1.36 (0.90)	15.6 (0.51)
460	1.34 (0.19)	3.59 (0.02)	0.57 (0.02)	19.5 (0.11)	3.07 (2.58)	5.14 (0.10)	2.70 (0.85)	15.5 (0.57)
480	1.05 (0.16)	3.59 (0.02)	0.59 (0.01)	19.9 (0.12)	2.55 (1.59)	5.31 (0.07)	2.56 (0.61)	15.4 (0.46)
530	1.12 (0.13)	3.62 (0.02)	0.59 (0.01)	20.4 (0.09)	1.85 (1.68)	5.35 (0.22)	1.11 (0.34)	16.2 (0.48)
580	1.15 (0.18)	3.59 (0.02)	0.62 (0.02)	20.1 (0.12)	2.52 (1.54)	5.27 (0.17)	2.66 (0.82)	14.9 (0.30)
680	1.61 (0.16)	3.56 (0.01)	0.65 (0.02)	19.8 (0.12)	1.51 (0.61)	5.11 (0.44)	5.10 (0.97)	14.6 (0.80)
780	1.05 (0.16)	3.51 (0.02)	0.63 (0.02)	19.8 (0.14)	2.88 (0.97)	5.07 (0.09)	5.08 (0.76)	14.4 (0.68)

band gap.[22] The two interband transitions obtained by unpolarized reflectance spectra at room temperature are 3.38 eV and 4.22 eV,[13] which are close to the previous data within reasonable experimental error.

From Fig. 4(a), the variation of both E_{cp1} and E_{cp2} can be separated into five parts: Part i to Part v for E_{cp1} and Part I to V for E_{cp2}, resembling the band gap results for PZT materials observed by Deineka *et al.* except for the additional parts (Part iii and Part III) occurring at ~400 K. The AFE phase, which is not observed in PZT materials but confirmed by the aforementioned XRD analysis in PLZST, can be interpreted as the additional part. The first four parts were linearly fitted, and the temperature coefficients of E_{cp1} are 2.45×10^{-4} eV/K, 1.85×10^{-3} eV/K, 1.90×10^{-4} eV/K, and 1.43×10^{-3} eV/K for Parts i to iv, respectively. As for E_{cp2}, the coefficients are 2.08×10^{-4} eV/K, 5.47×10^{-3} eV/K, 9.88×10^{-4} eV/K, and 7.82×10^{-3} eV/K from Parts I to IV, respectively. The values

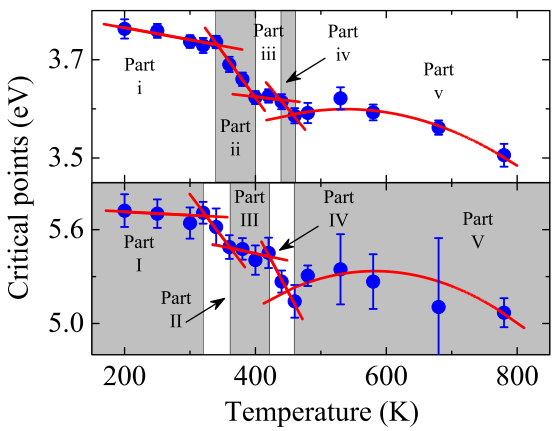

FIG. 4. Temperature dependence of the two critical-point energies, E_{cp1} (a) and E_{cp2} (b). The solid lines are linearly and quadratically fitted results. The gray regions indicate different phase transition behavior.

of Part i (I) and Part iii (III) are typical values for Pb-based materials.[12] However, the values of Part ii (II) and Part iv (IV) are large. The FE-AFE and AFE-PE transitions are suggested to undergo across these two parts, which agree well with previous electric experiments.[8] The last parts of E_{cp1} and E_{cp2} show nonlinear temperature dependence with maxima at ~536 K (E_{cp1}) and ~575 K (E_{cp2}), which can be attributed to the decomposition of PbO_2 to Pb_3O_4.[23]

To shed light on the variation of the CP energies, the microstructure should be considered. The ABO_3 perovskite structure is a three-dimensional network of regular corner-linked BO_6 octahedra with small B cations at the center of each octahedron and larger A cations centrally located in the AO_{12} cuboctahedral cavity formed by eight octahedra. The tolerance factor: $t = (r_A + r_O)/\sqrt{2}(r_B + r_O)$, where r_A, r_B, and r_O are the ionic radii of the A, B, and O ions, respectively, is less than one.[24] PLZST has A-site driven ferroelectricity, which is similar to the parent system (PZT). In the ideal cubic structure (high temperature side), the A-site (Pb) cations are on a site that is larger than the sum of the Pb and O ionic radii. The covalency between Pb and O increases the Born effective charges and thereby enhances dipolar interactions. These tip the balance in favor of ferroelectric instability, in which each Pb is off-center with respect to its cage of 12 surrounding O ions. For the A-site driven instability, it is important for the lattice to be highly polarizable, including the BO_6 octahedra. This results in off-centering of the B-site cations in response to the Coulomb potential of the off-centered Pb cations.[25] In the present work, the off-centering of Pb (A-site) could explain the variation of the transition E_{cp1}, which is assigned as the transition from O p and Pb s states to Pb 6p-like states. Part iv, which can be interpreted as the transition from PE to narrow AFE phase, suggests that the Pb off-centering is probably anisotropic or antiparallel. This can induce the small polarizability of the octahedra. With further cooling, the large slope of the transition E_{cp1} in Part ii indicates that the oriented Pb off-centering is followed by the large polarizability of the octahedra. The aforementioned two transitions can also be determined from the variation of E_{cp2}, which is assigned as the transition from nearly O p states to B ion d states and could contribute to the off-centering of the B-site cations. Part II and Part IV correspond to the large and small polarizability of the octahedra, respectively. It is worth noting that the total PT region of transition E_{cp2} (Parts II, III, and IV) is broader than that of E_{cp1} (Parts ii, iii, and iv). This relaxed behavior of E_{cp2} originates from the A-site driven mechanism. The influence of the off-centering from A-site cations is more nominal than that of the off-centering of B-site cations, which would result in less relaxed variation of the critical point. Furthermore, the influence of off-centering from A-site cations takes effort in prior to that of off-centering from B-site cations on cooling. This could be the reason for the difference between the PT temperature regions of E_{cp1} and E_{cp2}.

In summary, the phase transition of $(Pb_{0.97}La_{0.02})(Zr_{0.42}Sn_{0.40}Ti_{0.18})O_3$ ceramic has been investigated using temperature-dependent XRD and SE measurements. The transition from rhombohedral to tetragonal symmetry was confirmed. The variation of critical point energies obtained from fitting the second derivative of numerically inverted complex dielectric functions reveals the transition processes of both PE-AFE and AFE-PE. The electronic structure variation directly confirms the A-site driven mechanism of Pb-based materials.

One of the authors (X.C.) would like to thank Dr. Lin Sun for XRD measurements and Liping Xu, and Ting Huang for technical support. This work was financially supported by the Major State Basic Research Development Program of China (Grant Nos. 2011CB922200 and 2013CB922300), the Natural Science Foundation of China (Grant Nos. 11374097, 61376129, 11074076, and 61106122), Projects of Science and Technology Commission of Shanghai Municipality (Grant Nos. 13JC1402100, 13JC1404200, and 11520701300), and the Program for Professor of Special Appointment (Eastern Scholar) at Shanghai Institutions of Higher Learning.

[1]A. S. Mischenko, Q. Zhang, J. F. Scott, R. W. Whatmore, and N. D. Mathur, Science **311**, 1270 (2006).
[2]M. Ahart, M. Somayazulu, R. E. Cohen, P. Ganesh, P. Dera, H. K. Mao, R. J. Hemley, Y. Ren, P. Liermann, and Z. Wu, Nature **451**, 545 (2008).
[3]N. N. Luo, Y. Y. Li, Z. G. Xia, and Q. Li, Cryst. Eng. Comm. **14**, 4547 (2012).
[4]G. H. Haertling, J. Am. Cream. Soc. **82**, 797 (1999).
[5]R. E. Cohen, Nature **358**, 136 (1992).
[6]J. Zhang, Z. Yin, and M. S. Zhang, Appl. Phys. Lett. **81**, 4778 (2002).
[7]D. Berlincourt, IEEE Trans. Sonics Ultrason. **13**, 116 (1966).
[8]H. L. Zhang, X. F. Chen, G. Yu, F. Cao, C. L. Mao, G. S. Wang, X. L. Dong, and Y. L. Wang, Ferroelectrics **402**, 150 (2010).
[9]H. L. Zhang, X. F. Chen, F. Cao, G. S. Wang, X. L. Dong, Y. Gu, H. L. He, and Y. S. Liu, J. Appl. Phys. **108**, 086105 (2010).
[10]S. G. Choi, R. Chen, C. Persson, T. J. Kim, S. Y. Hwang, Y. D. Kim, and L. M. Mansfield, Appl. Phys. Lett. **101**, 261903 (2012).
[11]S. G. Choi, J. Hu, L. S. Abdallah, M. Limpinsel, Y. N. Zhang, S. Zollner, R. Q. Wu, and M. Law, Phys. Rev. B **86**, 115207 (2012).
[12]Z. H. Duan, Z. G. Hu, K. Jiang, Y. W. Li, G. S. Wang, X. L. Dong, and J. H. Chu, Appl. Phys. Lett. **102**, 151908 (2013).
[13]X. Chen, K. Jiang, Z. G. Hu, X. F. Chen, G. S. Wang, X. L. Dong, and J. H. Chu, Appl. Phys. Lett. **101**, 011914 (2012).
[14]Y. Li, Q. Li, L. Wang, Z. Yang, and X. Chu, J. Cryst. Growth **318**, 860 (2011).
[15]Y. Li, Q. Li, Q. Yan, Y. Zhang, X. Xi, X. Chu, and W. Cao, Appl. Phys. Lett. **101**, 132904 (2012).
[16]T. D. Kang, H. Lee, G. Xing, N. Izumskaya, V. Avrutin, B. Xiao, and H. Morkoç, Appl. Phys. Lett. **91**, 022918 (2007).
[17]C. M. Herzinger and B. D. Johs, U.S. Patent No. 5,796,983 (18 August 1998).
[18]P. Lautenschlager, M. Garriga, L. Viña, and M. Cardona, Phys. Rev. B **35**, 9174 (1987); **36**, 4821 (1987).
[19]W. L. Warren, J. Robertson, D. Dimos, B. A. Tuttle, G. E. Pike, and D. A. Payne, Phys. Rev. B **53**, 3080 (1996).
[20]H. Lee, Y. S. Kang, S. Cho, B. Xiao, H. Morkoç, T. D. Kang, G. S. Lee, J. Li, S. Wei, P. G. Snyder, and J. T. Evans, J. Appl. Phys. **98**, 094108 (2005).
[21]O. Gubanova and D. E. Ellis, Ferroelectrics **150**, 227 (1993).
[22]Z. Zhang, P. Wu, K. Ong, L. Lu, and C. Shu, Phys. Rev. B **76**, 125102 (2007).
[23]A. Deineka, L. Jastrabik, G. Suchaneck, and G. Gerlach, Ferroelectrics **273**, 155 (2002).
[24]M. Ghita, M. Fornari, D. J. Singh, and S. V. Halilov, Phys. Rev. B **72**, 054114 (2005).
[25]M. D. Johannes and D. J. Singh, Phys. Rev. B **71**, 212101 (2005).